the signal. The significance of these estimates was tested against nonoverlapping 45-year-long slices of data derived from the control run, i.e., against the hypothesis that the heat-content changes in the anthropogenic runs could have occurred as a result of natural, internal variability in the absence of any anthropogenic forcing. Forty-five-year chunks of the control run data were processed just as the observations and five anthropogenic realizations were processed, and then projected onto the signal. The results show that the signal strengths of the five realizations and observations are quantitatively similar and nonzero relative to the uncertainty of the natural variability of the model, i.e., the model and observed

projections are statistically consistent and not expected to occur as a result of internal model variability. The confidence associated with this statement exceeds 95%. With no variance weighting, i.e., nonoptimal detection, the results were essentially identical, if not a little stronger than in the optimal case.

32. B. Reichert, L. Bengtsson, R. Schnur, in preparation.
33. Supported by the National Oceanographic and Atmospheric Association Climate Change Data and Detection program and the U.S. Department of Energy, Office of Energy Research, as part of the International ad hoc Detection Group effort. Additional support from the U.S. Department of Energy (grant DE-FG03-98ER62505), the National Science Foundation (grant ATM-9901110), and the Scripps Institution is gratefully acknowledged. R.S. was partially supported by the European Commission under contract ENV4-CT97-0501. We are particularly indebted to the PCM group, headed by W. Washington, for their assistance and generosity with their model data and to S. Levitus and co-authors, whose earlier work gave rise to this study. Technical discussions with M. Allen, T. Delworth, and anonymous reviewers greatly improved the manuscript.

Climate Response to Orbital Forcing Across the Oligocene-Miocene Boundary

James C. Zachos,[1]* Nicholas J. Shackleton,[2] Justin S. Revenaugh,[1] Heiko Pälike,[2] Benjamin P. Flower[3]

Spectral analyses of an uninterrupted 5.5-million-year (My)–long chronology of late Oligocene–early Miocene climate and ocean carbon chemistry from two deep-sea cores recovered in the western equatorial Atlantic reveal variance concentrated at all Milankovitch frequencies. Exceptional spectral power in climate is recorded at the 406-thousand-year (ky) period eccentricity band over a 3.4-million-year period [20 to 23.4 My ago (Ma)] as well as in the 125- and 95-ky bands over a 1.3-million-year period (21.7 to 23.0 Ma) of suspected low greenhouse gas levels. Moreover, a major transient glaciation at the epoch boundary (~23 Ma), Mi-1, corresponds with a rare orbital congruence involving obliquity and eccentricity. The anomaly, which consists of low-amplitude variance in obliquity (a node) and a minimum in eccentricity, results in an extended period (~200 ky) of low seasonality orbits favorable to ice-sheet expansion on Antarctica.

Orbital dynamics are thought to have driven Quaternary climate change, but their effects in earlier times when climate boundary conditions differed have been difficult to resolve. Here, we examine the late Oligocene and early Miocene (~20.0 to 25.5 Ma), a time when Antarctica was either ice-free or only partially glaciated, using a 5.5-My-long high-fidelity benthic foraminiferal stable isotope record. This record is a composite constructed largely with newly collected data from Ocean Drilling Program (ODP) Site 926, Ceara Rise (3°43'N, 42°54'W), as well as data from Site 929. Sedimentation rates at Site 926, which is located at a depth of 3598 m where carbonate dissolution is reduced, are as much as 50% higher than at Site 929 and other deeper sites (1).

We use the age model of Shackleton and

colleagues (2) for our isotope records. They calibrated proxy records of Oligocene and Miocene lithologic cycles, including magnetic susceptibility (MS), in the Leg 154 cores (3) to an orbital curve (4) using modern values for tidal dissipation and dynamical ellipticity (5). They achieved an absolute calibration by pattern matching the 400-ky cycles of eccentricity-modulated precession in MS with similar cycles in the target curve. They then used individual obliquity maxima to establish the fine-scale tuning and verified this by comparing the 1.2-My amplitude modulation of obliquity in the data. The astronomical age derived for the Oligocene-Miocene (O/M) boundary, as recognized by the presence of *Sphenolithus delphix* and a positive carbon isotope anomaly of 0.65‰, is roughly 700 ky younger than that established in the radiometric calibrated time scale (6).

We developed high-resolution (~3.7 ky) carbon and oxygen isotope records for benthic foraminifera specimens collected from Hole 926B (7). Our records match those for Hole 929A (8) for each cycle down to the obliquity level over the interval of overlap (926B, 20.0 to 25.2 Ma; 929, 20.5 to 25.4 Ma) (Fig. 1A). The only no-

ticeable differences are the higher frequency oscillations present in the 926 record (e.g., precession) that are not resolved at Site 929 because of lower sedimentation rates (26 m/My for Hole 926B versus 19 m/My for Hole 929A across the O/M boundary). The ranges of isotope values are similar despite the nearly 1 km difference in water depth between sites. This similarity implies that the deep water in this part of the Atlantic was chemically homogeneous over much of this period and that a large portion of the variance in the isotopic record is signal.

The most prominent feature of the records is a positive excursion in $\delta^{18}O$ coupled with a positive shift in $\delta^{13}C$ values at 23.0 Ma, the Mi-1 excursion. This event, which can be distinguished in other deep-sea $\delta^{18}O$ records (9), is characterized by a series of obliquity period cycles beginning at 23.3 Ma over which $\delta^{18}O$ increase, to a peak at ~23.0 Ma. This peak is followed by a series of three declining cycles (deglaciations) over the next ~150,000 years. Thereafter, the cycles appear to be predominantly 100 ky. A second, but weaker, positive $\delta^{18}O$ excursion occurs at 21 Ma. The $\delta^{13}C$ values show low-frequency cycles that increase in amplitude and value, eventually peaking from 23.0 to 21.6 Ma, after which they decline.

To ascertain the nature of the high-frequency signals in the isotope records, we first built composite $\delta^{18}O$ and $\delta^{13}C$ time series by splicing gaps in the Hole 926B records with grafts from the Hole 929A records [Web table 1 (10)]. We then applied band-pass gaussian filters to each isotope record as well as the orbital calculations and MS to extract oscillations associated with 400-, 100-, and 41-ky cycles [AnalySeries (11)] (Fig. 1B). In the 400-ky band, both the $\delta^{13}C$ and $\delta^{18}O$ filters co-vary with the 400-ky filter of eccentricity, in that they appear phase-locked between 20 to 24 Ma. Also, the 400-ky eccentricity-related amplitude modulation of $\delta^{13}C$, and to a lesser extent $\delta^{18}O$, exhibits a pattern similar to that of the orbital modulation, including subtle peaks near ~21.4 and 23.0 Ma (Fig. 1B). The amplitude of the 400-ky filter of $\delta^{18}O$ increases only after 23.4 Ma, just below the O/M boundary. This is the

[1]Earth Sciences Department, Center for Dynamics and Evolution of the Land-Sea Interface, University of California, Santa Cruz, CA 95064, USA. [2]Godwin Laboratory for Quaternary Studies, Cambridge University, Cambridge CB2 3SA, UK. [3]College of Marine Science, University of South Florida, St. Petersburg, FL 33701, USA.

*To whom correspondence should be addressed. E-mail: jzachos@es.ucsc.edu

opposite of the pattern in MS. The amplitude modulation of the 100-ky filter of $\delta^{18}O$ also matches that of the orbit, particularly from 23.0 to 21.7 Ma when the mean amplitude exceeds that in previous and subsequent intervals.

Evaluation of variance in the isotope time series in the frequency domain by spectral analyses (12) revealed spectral power concentrated at all the primary Milankovitch frequency bands (Fig. 2A): obliquity (41 ky), eccentricity (95, 125, and 406 ky), as well as precession (19, 23 ky), which was not resolved by the Site 929 spectra. Additional power can be seen in the 54-ky band for $\delta^{13}C$. To evaluate the patterns of frequency change in the time domain, we constructed evolutive spectra for each variable, including MS (Fig. 3). Variance is concentrated at the 41-ky period in both isotope series and MS. Modulation of the obliquity amplitude and frequency at a 1.25 My period is prominent in MS but can be seen in the $\delta^{13}C$ data as well. Power at the eccentricity frequencies (95, 125, and 406 ky), which is weak in MS, builds and declines on lower frequency cycles in the isotope records. For example, low-frequency power in the $\delta^{13}C$ series appears to alternate between the two eccentricity band frequencies (100 and 400 ky) roughly every 2.3 My, whereas in the $\delta^{18}O$ series it is persistent at both frequencies between 20 and 23 Ma, but only in the 100-ky band between 23.0 and 25.5 Ma. Also, as revealed by filtering, the concentration of power in the $\delta^{18}O$ data at the 125- and 95-ky frequency bands is greatest between 21 to 23 Ma and modulates in a similar manner to the orbital elements.

Cross-spectral analysis shows that the $-\delta^{18}O$ record is highly coherent with eccentricity in each frequency band. The minima in $\delta^{18}O$ lag maxima in eccentricity by 31 to 6 ky for the 400- and 125-ky periods, respectively (Fig. 2B and Table 1). The relations between $-\delta^{13}C$ and the orbits are similar, although the phase lags are larger: 56 and 16 ky, respectively. In view of the residence time ($\sim10^5$ years) of carbon in the ocean, these phase relations are consistent with the notion that orbital forcing of climate leads, and perhaps drives, changes in the ocean carbon budget. The phase relations in the obliquity band (not plotted) reveal high coherency for $-\delta^{18}O$ at 41 ky with a lag of 3 ky ($\sim25°$) and slightly weaker coherency at 54 ky with a similar phase relation ($\sim30°$). The phase angle of $-\delta^{13}C$ values, on the other hand, is $-165°$, or essentially 180° opposite that of $\delta^{18}O$.

Complex demodulation of the detrended $\delta^{18}O$ record of eccentricity and the orbital calculation were performed using the method of Park and Maasch (13). This analysis reveals a close correlation (r = 0.6) between the amplitude modulation of the 100-ky ec-

centricity signal and that of the oxygen isotopes [Web fig. 1 (10)], and cross-spectral analysis of the amplitude modulation shows a coherent phase structure, particularly from 21.0 to 23.4 Ma. In addition to supporting the precision of the independent orbital tuning, these findings indicate a persistent and strong link between eccentricity forcing and climatic response.

Several independent lines of evidence suggest that Antarctica was at least intermittently glaciated, though never fully ice-covered, during the latest Oligocene and early Miocene (14–16). For the 400-ky period cycles including Mi-1, the observation of co-

eval oscillations in planktonic $\delta^{18}O$ values with half the amplitude observed in the benthic $\delta^{18}O$ suggests that roughly 50% of the signal is ice-volume related (8). We thus interpret higher benthic $\delta^{18}O$ as reflecting a combination of cooler temperatures and greater Antarctic ice volume (17).

On the basis of coherency patterns and phase relations, we find that all early Miocene eccentricity minima coincide with episodes of deep-sea cooling and increased ice volume, as indicated by the $\delta^{18}O$ record. The same also appears to be the case for the obliquity cycles. This suggests that for ice to accumulate on Antarctica in the early Mio-
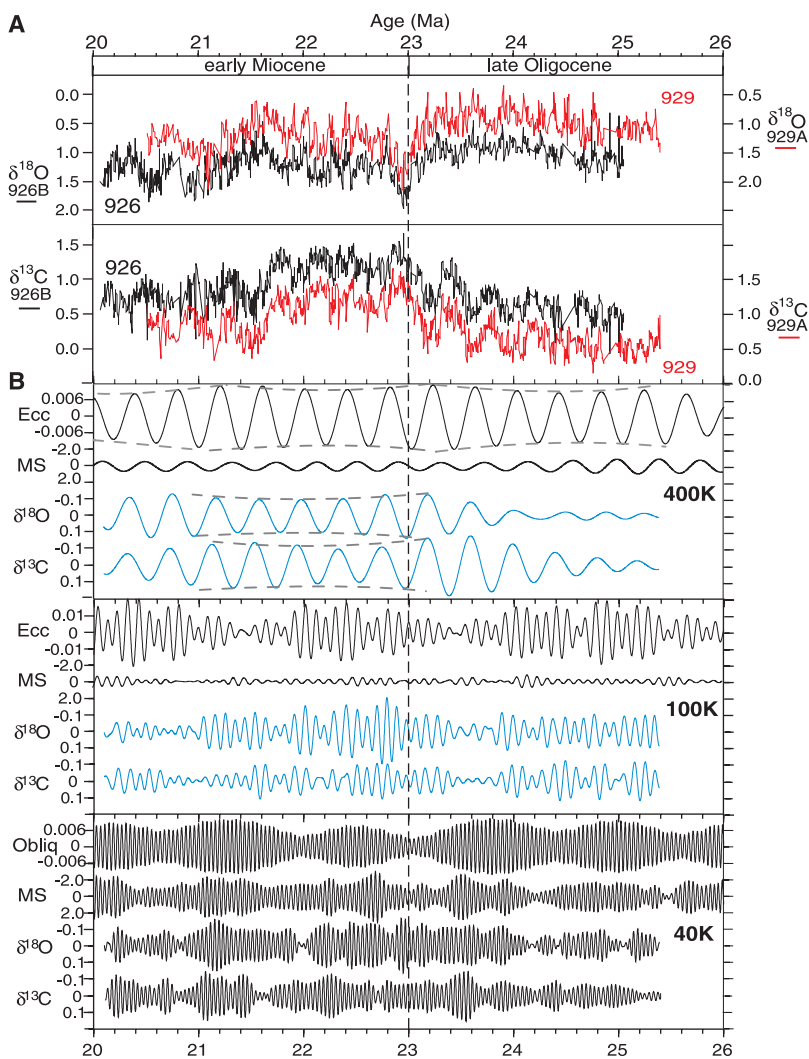
Fig. 1. (A) The Hole 926B benthic foraminifer $\delta^{13}C$ and $\delta^{18}O$ records (vPDB) plotted versus astronomical age. Also plotted (with axes offset by 0.5‰) are the equivalent records from Hole 929A (8). The isotope values (vPDB) are based on analyses of benthic taxa *Cibicidoides mundulus* (7). Both $\delta^{18}O$ axes are reversed (negative up). **(B)** Band-pass filters of the composite Oligocene-Miocene isotope time series designed to isolate oscillations with periods of 41, 100, and 400 ky. The central frequencies and bandwidths of the filters are 0.025 ± 0.005, 0.010 ± 0.003, and 0.0025 ± 0.0005, respectively. The axes of the $\delta^{18}O$ and $\delta^{13}C$ filters are reversed. For the isotope composite, splices from the Hole 929A record are used to fill gaps in the Hole 926B record (10). Most of the splices were short, bridging gaps of less than 50 ky, primarily in the unrecovered coring gaps in Hole 926B. The exceptions are an unsampled interval from 20.8 to 21.1 Ma and an unrecovered interval centered at 24.5 Ma. The composite series was then resampled (Δt = 1 ky, n = 5290) before filtering and other analyses. Filters with identical central frequencies and bandwidths are shown for the orbital eccentricity and obliquity curves (4) and for the composite magnetic susceptibility.

cene, the ideal situation is one in which the seasonal extremes (precession and obliquity) are reduced, or more importantly, the summer temperatures are consistently cool. We speculate that for a polar continent, at least during the early Miocene, it is the lack of warm summers that permits ice sheets to expand; winter temperatures are less important.

The long eccentricity period (400 ky) is present but weak in the climatic spectrum of the late Pliocene and Pleistocene (*18, 19*). In the latest Oligocene, power in the $\delta^{18}O$ record at the 400-ky period is also weak, but doubles between 23 to 24 Ma, even though the eccentricity signal remains relatively constant. Why would sensitivity to forcing at this frequency suddenly increase during the early Miocene? The answer may lie in the global carbon cycle and atmospheric pCO_2, the cycling of which is partially reflected in the $\delta^{13}C$ data. The increase in amplitude of $\delta^{18}O$ variation is preceded by an increase in the amplitude of the $\delta^{13}C$ 400-ky cycle, as well as by a rise in the long-term mean (*8*). Both changes hint at a change in one or several of the major fluxes in the global carbon cycle, most likely an increase in the rate of reduced carbon burial, and/or a decrease in the rate of mantle out-gassing of CO_2 (*20*).

The initial rise in amplitude of the 400-ky $\delta^{13}C$ cycles precedes that in $\delta^{18}O$ by ~1 My. This implies that the observed oscillations in $\delta^{13}C$ and the carbon cycle are being paced or driven by climate cycles, but possibly feeding back into climate over both the short and long term. Similar 400-ky oscillations in $\delta^{13}C$ values observed in other intervals of the early Cenozoic are thought to arise from variations in marine organic carbon burial as influenced by climate, and its attendant effects on atmospheric and ocean circulation and the carbon cycle (*21–24*). The constant phase relation between $\delta^{13}C$ and eccentricity supports the notion that there is a coupling between climate and the carbon cycle. The cause of the late Oligocene rise in cycle amplitude or sensitivity to this pacing is unknown. It might have been caused by a large-scale reorganization of ocean circulation patterns (*25, 26*) or by tectonic changes. It is also possible that signal amplification originated in the low latitudes through eccentricity-modulated precession (*27, 28*), although at present it is unclear what the nature of this coupling would be. In any case, our data show that a system sensitivity shift did occur, and that it was preceded by a major change in the operation of the carbon cycle.

Likewise, a reduction in atmospheric pCO_2 levels may explain the period of heightened sensitivity to eccentricity forcing, which is reflected in the relative increase in amplitude of the 100-ky cycles between 21.7 and 23.0 Ma. This is also the time when the coherence with eccentricity is at a maximum in terms of phase and amplitude. Because this coincides with the period of high $\delta^{13}C$ values, it suggests that the system sensitivity (e.g., ice volume) to eccentricity-modulated precession is heightened when pCO_2 is low. The inference of a reduction in pCO_2 from the carbon isotopes is consistent with proxy
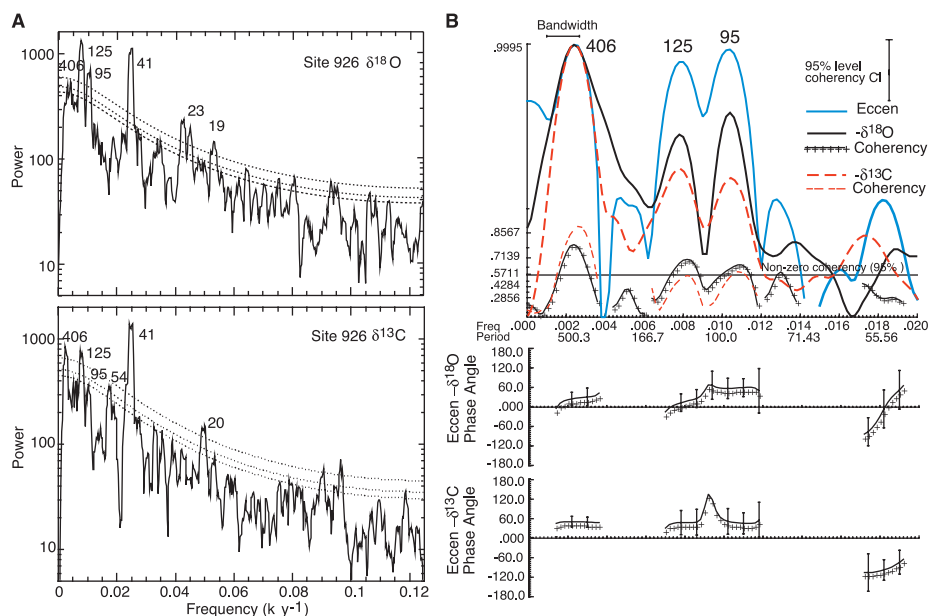
Fig. 2. (**A**) Log-power spectrum of the composite $\delta^{13}C$ and $\delta^{18}O$ time series determined by the multi-taper method (MTM) with robust red noise background for the significance calculation (*36*). The 10, 5, and 1% significance levels are indicated by dotted lines (confidence intervals of 90, 95, and 99%). The time series was detrended before analysis using a running mean filter, which provides better resolution of the low frequencies than a linear detrend. The Milankovitch frequencies are all represented and significant. Some of the suborbital spectra are marginally significant. (**B**) Log-variance cross spectrum, coherency, and phase of the $\delta^{18}O$ and $\delta^{13}C$ composites relative to the orbital spectrum obtained by cross-spectral analysis (Arand program). Following convention and to be consistent with the orientation of axes in Fig. 1B, the analyses are carried out on the inverse of both $\delta^{18}O$ and $\delta^{13}C$ relative to the orbital spectrum. The number of lags was set to 800 for analysis of eccentricity frequencies (bandwidth = 0.00166) and 500 for obliquity (results shown in Table 1) with a 95% confidence interval. The maximum frequency is set to 0.02 ky^{-1} to highlight the relations at the eccentricity frequency bands. For coherency and phase, points are shown only where cross-spectral density exceeds 1% of the maximum.
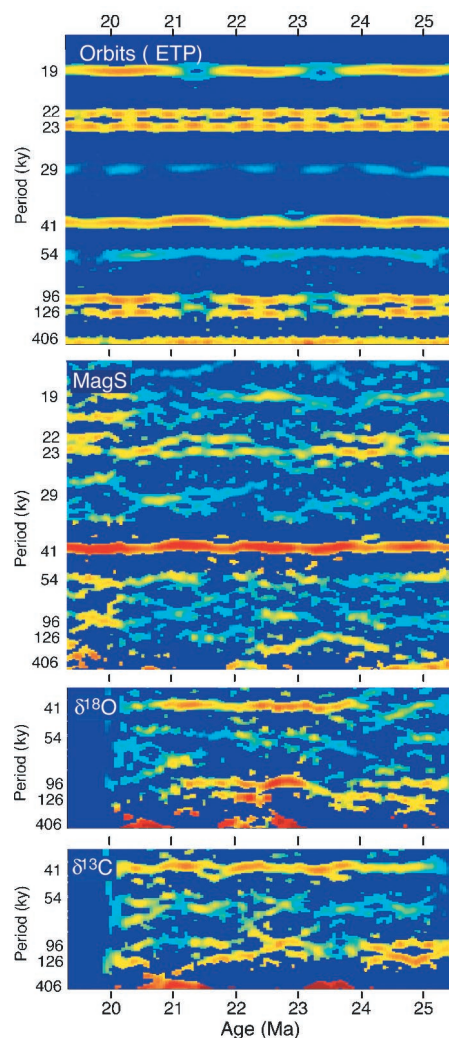
Fig. 3. Evolutive spectra for eccentricity, obliquity (tilt), and precession (ETP) (*4*) magnetic susceptibility, and the $\delta^{18}O$ and $\delta^{13}C$ composites with periods plotted on the left axes. The analysis is based on the Thomson multitaper method with a time-bandwidth product of 4, eigenspectra of 6, a sliding window length of 750 ky, and a step size of 50 ky. Because of the relative weakness of the higher frequency signals in this analysis, the plots for $\delta^{13}C$ and $\delta^{18}O$ time series are terminated above the obliquity frequency. The figure shows how the distribution of signal power in the MS and isotope time series varies with time relative to the orbits.

records that show a mid-Cenozoic decline in pCO_2 across the O/M boundary (*29, 30*). A similar mechanism has also been called upon to explain the onset of the 100-ky cycles in the late Pleistocene (*31*).

The Mi-1 event stands out as a rare climatic anomaly; it precisely coincides with a major epoch boundary marked by accelerated turnover of several groups of marine and terrestrial biota (*32*). The magnitude of the excursion suggests the brief appearance of a full-scale ice sheet on east Antarctica coupled with a few degrees of deep-sea cooling. The high $\delta^{18}O$ values at the peak of the excursion (~2.2‰) are consistent with a global ice volume equivalent to that of the late Miocene.

Mi-1 coincides with a period of low eccentricity associated with the 400-ky cycle, but one that is no more extreme than previous and subsequent eccentricity minima (Fig. 4A). What is unusual about the orbits is an extended period of low-amplitude variability in obliquity at approximately the same time, during which obliquity varied between 0.398 and 0.414 rad, or 22.80° to 23.72° (Fig. 4B). These nodes in obliquity are a regular feature of the low-frequency (period ~ 1.25 My) amplitude modulation of obliquity and have already been implicated for driving late Miocene glacial cycles (*33*). The obliquity node
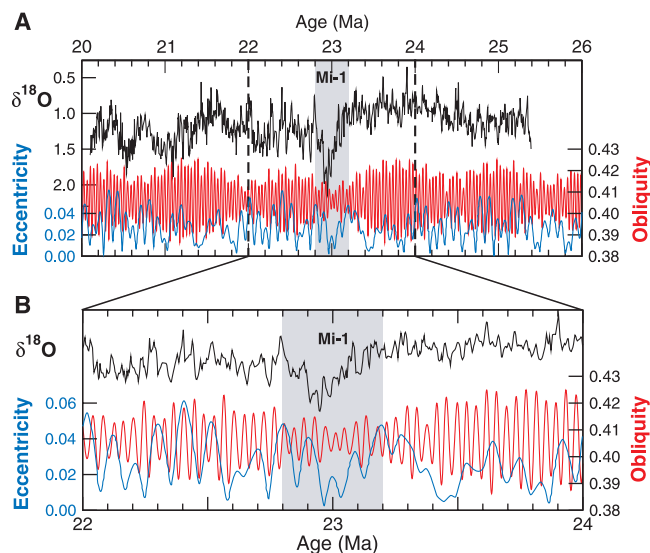
at 23.0 Ma, however, is longer than previous or subsequent nodes over the period 20 to 26 Ma by at least two obliquity cycles. The congruence of this node with an eccentricity minimum would have placed the planet in a position of sustained unusually low seasonal variability, with reduced extremes of warmth and coldness. We propose that during the early Miocene, a time when the Antarctic continent was only partially glaciated, accumulation of ice would have been limited by the "warm summer" orbital configurations (e.g., high obliquity). Beginning at 23.2 Ma, as eccentricity and the amplitude of obliquity declined, polar summers were consistently cooler and ice-sheets expanded until 23.0 Ma. After this time, as eccentricity rapidly increased, this process reversed, resulting in a rapid step-like reduction in ice-volume. Subsequent nodes in obliquity, which do not correspond with prolonged eccentricity minima, do not result in extreme glaciations.

The Mi-1 event also marks a fundamental shift in the climate system as evident in the ~0.4‰ jump in the baseline $\delta^{18}O$ values of benthic foraminifers from the late Oligocene to early Miocene and in the rise in the amplitude of the 406-ky cycles (Fig. 1). This, and a gradual rise in mean ocean carbon isotope values preceding Mi-1, suggests that at 23.0 Ma the ocean or atmosphere system

crossed a climatic threshold, switching to a new mode. This system reorganization may have triggered positive feedbacks from the carbon cycle, thereby creating a brief overshoot of equilibrium (*34*). The pronounced carbon isotope enrichment approaching the boundary supports this hypothesis because it is consistent with a major shift in the nature or rate of carbon cycling. The exact cause of the carbon cycle perturbation is unknown. Nonetheless, the climatic response to the orbital anomaly would have been further enhanced by this feedback.

Other Neogene glacial episodes, including the onset of Northern Hemisphere glaciation in the early Pleistocene, have been attributed to low-frequency secular changes in the amplitude of obliquity (*33, 35*). The data presented here, however, indicate that eccentricity-modulated variations in precession must contribute as well, at least during the early Miocene. In examining the orbital curves, we have identified at least two other intervals when low-amplitude nodes align with low eccentricity at 18.2 and 27.0 Ma. Although those nodes are not as long as at 23.0 Ma, characterization of climatic anomalies at these two times would substantiate the orbital anomaly hypothesis, while also serving to confirm the orbital solutions.

References and Notes

1. W. B. Curry *et. al.*, *Init. Rep., Proc. Ocean Drill. Prog.* (Ocean Drilling Program, College Station, TX, 1995), vol. 154.
2. N. J. Shackleton, S. J. Crowhurst, G. P. Weedon, J. Laskar, *Philos. Trans. R. Soc. London Ser. A* **357**, 1907 (1999).
3. Magnetic susceptibility, color reflectance and natural gamma records all reflect variations in the ratio of terrigenous matter to carbonate in the sediment. Orbital tuning made use of all these properties, which were measured at 2.5-cm intervals in each core.
4. J. Laskar, F. Joutel, F. Boudin, *Astron. Astrophys.* **270**, 522 (1993).
5. H. Pälike, N. J. Shackleton, *Earth Planet. Sci. Lett.* **182**, 1 (2000).
6. N. J. Shackleton, M. A. Hall, I. Raffi, L. Tauxe, J. Zachos, *Geology* **28**, 447 (2000).
7. ODP Hole 926B was sampled at 10-cm intervals from 404 to 552 m composite depth (cores 41 to 56x). Roughly 15 g of sediment were collected, freeze-dried, weighed, and disaggregated in a sodium hexametaphosphate solution (~50°C) on an orbital shaker. The samples were wet-sieved (>63 μm), dried, weighed, and picked for benthic foraminifera taxa *Cibicidoides mundulus*. Stable isotope measurements for each level were made on two to eight specimens combined using an Autocarb preparation system coupled to a PRISMIII gas source mass spectrometer. All values are reported in the per mil notation relative to Pee Dee Belemnite (vPDB). Standardization was established through analysis of NBS19 and Carrerra Marble (in-house).
8. H. A. Paul, J. C. Zachos, B. P. Flower, A. Tripati, *Paleoceanography* **15**, 471 (2000).
9. K. G. Miller, J. D. Wright, R. G. Fairbanks, *J. Geophys. Res.* **96**, 6829 (1991).
10. Web table 1 and Web fig. 1 are available at *Science* Online at www.sciencemag.org/cgi/content/full/292/5515/274/DC1.
11. D. Paillard, L. Labeyrie, P. Yiou, *EOS* **77**, 379 (1996).
12. Both the Multitaper and Blackman-Tukey (Arand software package) methods were used to evaluate the spectral density of the isotope records. The re-

Fig. 4. Gray area bounds the Mi-1 event as expressed in the $\delta^{18}O$ time-series relative to (**A**) the orbital eccentricity and obliquity (in rad) curves (*4*) over the period 20 to 26 Ma and (**B**) over the period 22 to 24 Ma. Mi-1 coincides with an interval of low eccentricity and an "extended" low-amplitude node in obliquity.

Table 1. Cross-spectral data (20 to 26 Ma).

Frequency (ky^{-1})	Period (ky)	Coherency	Phase angle (°)	Phase (ky)
		Eccentricity versus $-\delta^{18}O$		
2.50×10^{-3}	406	0.80	27.8 ± 19.0	31.0 ± 4.8
8.00×10^{-3}	125	0.71	18.5 ± 25.0	5.9 ± 0.6
1.05×10^{-2}	95	0.65	59.1 ± 28.0	15.6 ± 5.1
		Eccentricity versus $-\delta^{13}C$		
2.50×10^{-3}	406	0.88	50.4 ± 14.4	56.1 ± 15.7
8.00×10^{-3}	125	0.55	47.8 ± 35.0	16.6 ± 4.4
1.05×10^{-2}	95	0.60	46.7 ± 32.9	12.3 ± 3.2

sults were essentially identical, with the only difference being in the higher resolution and greater peak separation obtained with the Multitaper method.

13. J. Park, K. A. Maasch, *J. Geophys. Res.* **98**, 447 (1993).
14. R. M. Leckie, P. N. Webb, *Geology* **11**, 578 (1983).
15. W. Ehrmann, *Palaeogeogr. Palaeoclimatol. Palaeoecol.* **139**, 213 (1998).
16. L. Sagnotti, F. Florindo, K. L. Verosub, G. S. Wilson, A. P. Roberts, *Geophy. J. Int.* **134**, 653 (1998).
17. The δ¹⁸O values of *Cibicidoides* and most other benthic foraminifera taxa reflect on changes in both water temperature and ice-volume. For example, benthic δ¹⁸O will increase by 0.25‰ for each 1°C decline in temperature. On the other hand, a doubling of Antarctic ice-sheet mass would increase ocean (and benthic) δ¹⁸O by roughly 1.0‰.
18. S. C. Clemens, R. Tiedemann, *Nature* **385**, 801 (1998).
19. Although Pleistocene climate has a strong (dominant) 100-ky signal, the direct effects of eccentricity on global climate, particularly in polar regions, are considered too small to account for these changes. This and the lack of a similarly strong climate signal associated with the 400-ky eccentricity band, which has an equivalent ef-

fect on the radiation balance, are often viewed as major deficiencies of Milankovitch theory.
20. Marine organic carbon has a mean δ¹³C of −20‰, whereas mantle-derived CO_2 has a mean δ¹³C of −7‰. As a result, a sustained change in the flux of either has the potential to alter the mean δ¹³C of the ocean, as well as pCO_2, on 10⁴ to 10⁶ year time scales.
21. T. D. Herbert, *Proc. Natl. Acad. Sci. U.S.A.* **94**, 8362 (1997).
22. B. P. Flower, J. P. Kennett, *Palaeogeogr. Palaeoclimatol. Palaeoecol.* **108**, 537 (1994).
23. J. C. Zachos, B. P. Flower, H. Paul, *Nature* **388**, 567 (1997).
24. J. C. Zachos, T. M. Quinn, K. A. Salamy, *Paleoceanography* **11**, 251 (1996).
25. U. Mikolajewicz, E. Maierreimer, T. J. Crowley, K. Y. Kim, *Paleoceanography* **8**, 409 (1993).
26. G. T. Nong, R. G. Najjar, D. Seidov, W. H. Peterson, *Geophys. Res. Lett.* **27**, 2689 (2000).
27. D. A. Short, J. G. Mengel, T. J. Crowley, W. T. Hyde, G. R. North, *Quat. Res.* **35**, 157 (1991).
28. S. Rutherford, S. D'Hondt, *Nature* **408**, 72 (2000).

29. M. Pagani, M. A. Arthur, K. H. Freeman, *Paleoceanography* **14**, 273 (1999).
30. P. N. Pearson, M. R. Palmer, *Nature* **406**, 695 (2000).
31. M. E. Raymo, *Annu. Rev. Earth Planet. Sci.* **22**, 353 (1994).
32. E. N. Edinger, M. J. Risk, *Palaios* **9**, 576 (1994).
33. L. J. Lourens, F. J. Hilgen, *Quat. Int.* **40**, 43 (1997).
34. J. C. Zachos, K. C. Lohmann, J. C. G. Walker, S. W. Wise, *J. Geol.* **101**, 191 (1993).
35. M. A. Maslin, X. S. Li, M. F. Loutre, A. Berger, *Q. Sci. Rev.* **17**, 411 (1998).
36. M. E. Mann, J. M. Lees, *Clim. Change* **33**, 409 (1996).
37. We are indebted to M. Harvey for assistance in generating the Site 926 stable isotope record, and S. Crowhurst for assisting with the time series analyses and providing comments on this manuscript. We also thank B. Beitler, J. Chapmann, and G. Koehler for technical assistance and F. Hilgen and T. Crowley for feedback on the orbital alignment anomaly hypothesis. Supported by the National Science Foundation (EAR-9725789).

Molecular Mechanisms of the Biological Clock in Cultured Fibroblasts

Kazuhiro Yagita,[1] Filippo Tamanini,[2] Gijsbertus T. J. van der Horst,[2] Hitoshi Okamura[1]*

In mammals, the central circadian pacemaker resides in the hypothalamic suprachiasmatic nucleus (SCN), but circadian oscillators also exist in peripheral tissues. Here, using wild-type and *cryptochrome* (*mCry*)–deficient cell lines derived from *mCry* mutant mice, we show that the peripheral oscillator in cultured fibroblasts is identical to the oscillator in the SCN in (i) temporal expression profiles of all known clock genes, (ii) the phase of the various mRNA rhythms (i.e., antiphase oscillation of *Bmal1* and *mPer* genes), (iii) the delay between maximum mRNA levels and appearance of nuclear mPER1 and mPER2 protein, (iv) the inability to produce oscillations in the absence of functional *mCry* genes, and (v) the control of period length by mCRY proteins.

In the mouse, the core oscillator of the master circadian clock in the SCN is composed of interacting positive and negative transcription-translation feedback loops (*1–3*), which involve three homologs of the *Drosophila* gene *period* (*mPer1*, *mPer2*, and *mPer3*), two cryptochrome genes (*mCry1* and *mCry2*), and the transcriptional activator genes *Clock* and *Bmal1* (*1, 2, 4*). A key step in this feedback loop is the shutdown of CLOCK- and BMAL1-driven transcription by mCRY proteins (*4*). To keep pace with the solar day-night cycle, the master clock can be entrained by light received through photoreceptors in the retina (*5*). Molecular oscillators also exist

in peripheral tissues, where they cycle with a 6- to 8-hour delay with respect to the central pacemaker (*6–8*). In contrast to *Drosophila* and zebrafish, mammalian peripheral clocks do not directly respond to light but are synchronized by the SCN by neuronal and/or humoral signals (*9*). In vitro, brief treatment of cultured cells with various compounds [serum, forskolin, 12-*O*-tetradecanoylphorbol 13-acetate (TPA), adenosine 3′,5′-monophosphate (cAMP), or dexamethasone] induces rhythmic expression of the clock genes *Per1*, *Per2*, and *Cry1* and the circadian transcription factor gene *dbp* for two to three cycles (*6, 10–12*).

To investigate whether the molecular makeup of the peripheral oscillator in cultured fibroblasts resembles that of the core oscillator in the SCN, we determined the expression profiles of all known clock genes in cultured rat-1 fibroblasts over a period of 3 days (*13*). To trigger the oscillations, we used the vasocontracting peptide endothelin-1

(ET-1) (*14*), which activates the protein kinase C–mitogen-activated protein kinase cascade and cAMP response element–binding protein (CREB) phosphorylation (*15*). This treatment induces a rapid, robust increase in *Per1* and *Per2* gene expression, followed by a sharp reduction in corresponding mRNA levels and subsequent synchronous cycling of *Per1*, *Per2*, *Per3*, and *dbp* mRNAs (Fig. 1) (*16, 17*). Also, robust cycling of *Bmal1* mRNA was observed, with mRNA levels accumulating antiphase to *Per* and *dbp* mRNA cycles. *Clock* mRNA levels were constant at all time points examined. In addition, *Cry1* expression showed rhythmicity, peaking 4 to 8 hours after *Per* mRNAs (*16*). These data demonstrate that ET-1 can induce circadian gene expression in cultured rat-1 cells and that the temporal expression patterns of *Per*, *Bmal1*, *Cry1*, and *dbp* genes (all rhythmically expressed) as well as the *Clock* gene (constitutively expressed) match those in the SCN (*1, 18*). Casein kinase Iε (*CKIε*) and *Cry2* genes did not show apparent rhythmic expression in rat-1 cells, a finding consistent with the observation that in the SCN *CKIε* is constitutively expressed (*19*) and cycling of mouse *Cry2* is weak (*18*) or not detectable (*20*).

Next, we analyzed by immunocytochemistry the PER1 and PER2 protein expression profiles in these cells. Nuclear staining occurred 26 to 28 hours after treatment, indicating that mPER1 and mPER2 protein cycles follow the rhythm of *Per1* and *Per2* mRNA expression with a 4- to 8-hour delay (Fig. 2), as in the SCN (*21*). In addition, pronounced PER1 and PER2 nuclear staining was found 1.5 hours after ET-1 treatment (Fig. 2) (*22*), suggesting that ET-1 causes rapid synthesis of PER1 and PER2 and translocation of these proteins into the nucleus. This nuclear PER2 may up-regulate *Bmal1* expression and down-regulate *Per* gene expression 4 hours after ET-1 treatment (Fig. 1)

[1]Division of Molecular Brain Science, Department of Brain Sciences, Kobe University Graduate School of Medicine, Chuo-ku, Kobe 650-0017, Japan. [2]Center for Biomedical Genetics, Department of Cell Biology and Genetics, Erasmus University, Post Office Box 1738, 3000 DR, Rotterdam, Netherlands.

*To whom correspondence should be addressed. E-mail: okamurah@kobe-u.ac.jp